ADVANCED MATERIALS
www.advmat.de

Flash Recycling of Graphite Anodes

*Weiyin Chen, Rodrigo V. Salvatierra, John Tianci Li, Carter Kittrell, Jacob L. Beckham, Kevin M. Wyss, Nghi La, Paul E. Savas, Chang Ge, Paul A. Advincula, Phelecia Scotland, Lucas Eddy, Bing Deng, Zhe Yuan, and James M. Tour**

The ever-increasing production of commercial lithium-ion batteries (LIBs) will result in a staggering accumulation of waste when they reach their end of life. A closed-loop solution, with effective recycling of spent LIBs, will lessen both the environmental impacts and economic cost of their use. Presently, <5% of spent LIBs are recycled and the regeneration of graphite anodes has, unfortunately, been mostly overlooked despite the considerable cost of battery-grade graphite. Here, an ultrafast flash recycling method to regenerate the graphite anode is developed and valuable battery metal resources are recovered. Selective Joule heating is applied for only seconds to efficiently decompose the resistive impurities. The generated inorganic salts, including lithium, cobalt, nickel, and manganese, can be easily recollected from the flashed anode waste using diluted acid, specifically 0.1 M HCl. The flash-recycled anode preserves the graphite structure and is coated with a solid-electrolyte-interphase-derived carbon shell, contributing to high initial specific capacity, superior rate performance, and cycling stability, when compared to anode materials recycled using a high-temperature-calcination method. Life-cycle-analysis relative to current graphite production and recycling methods indicate that flash recycling can significantly reduce the total energy consumption and greenhouse gas emission while turning anode recycling into an economically advantageous process.

1. Introduction

The enablement of alternative energy sources relies heavily on commercial rechargeable batteries, especially lithium-ion batteries (LIBs), with high energy density (≈200 Wh kg^{-1}) and reliable stability.[1,4] This demand is being met by an ever-increasing production of batteries. By 2026, a five-fold increase in annual production capacity is expected relative to 2017.[5,6] This growth, although impressive, also projects a future in which critical metal sustainability (e.g., Li, Co, Ni) and the staggering accumulation of spent LIBs will be environmentally off-putting.[7] Effective recycling methods that can close the loop of the LIB lifecycle are needed. The current commercial LIB recycling methods, such as hydrometallurgical and pyrometallurgical processes,[8,9] mainly focus on recovering the valuable battery metals such as Li, Co, Ni, and Mn from the cathodes, while the anodes are either burned for energy or landfilled.[3] The anodes consist of battery-grade graphite, accounting for ≈20% of the total weight and ≈15% of the cost of LIBs. A feasible method for recycling the spent graphite anodes must be cost-effective and efficient to represent a viable recycling method. Recycled graphite powder could provide higher profit while minimizing the release of valuable metals to the environment.

Since the cost range for graphite anodes is \$8000–\$15 000 ton^{-1}, which is not as high as the cost range of the transition metal oxide cathode (\$20 000–\$50 000 ton^{-1} based on composition), industry has paid less attention to recycling anode waste.[5] On the laboratory scale, several graphite recycling processes have been proposed, such as a Fenton reagent-assisted flotation process involving Fe^{2+}/H_2O_2 to modify the surface,[10] hydrometallurgical methods followed by filtration,[11] a combined sulfuric acid curing, leaching and high temperature calcination process,[12] and a multistep heating and sintering method.[13] However, direct wet chemistries cannot eliminate the complex organic and inorganic impurities and they suffer from low efficiency. In addition, the use of strong acids [14,15] can contaminate the graphite and afford troublesome secondary waste streams. Other methods require continuous high temperature heating (2800–3500 K) to gasify the organic and inorganic wastes, while regenerating the graphite anode.[5] Prior work[16]

W. Chen, R. V. Salvatierra, J. T. Li, C. Kittrell, J. L. Beckham, K. M. Wyss, N. La, P. E. Savas, C. Ge, P. A. Advincula, P. Scotland, L. Eddy, B. Deng, Z. Yuan, J. M. Tour
Department of Chemistry
Rice University
6100 Main Street, Houston, TX 77005, USA
E-mail: tour@rice.edu
C. Ge, L. Eddy
Smalley-Curl Institute and Applied Physics Program
Rice University
6100 Main Street, Houston, TX 77005, USA
P. Scotland, J. M. Tour
Department of Materials Science and NanoEngineering
Rice University
6100 Main Street, Houston, TX 77005, USA
J. M. Tour
Smalley-Curl Institute
NanoCarbon Center and the Welch Institute for Advanced Materials
Rice University
6100 Main Street, Houston, TX 77005, USA

The ORCID identification number(s) for the author(s) of this article can be found under https://doi.org/10.1002/adma.202207303.

DOI: 10.1002/adma.202207303

has shown that supercritical or subcritical CO_2 was used to extract the electrolyte from the anode waste, followed by the thermal treatment to remove the other impurities with heating temperature of ≈1273 K for ≈5 h, which achieves the recovery of the electrolyte and the rejuvenation of the graphite anode during the process. Therefore, high temperature calcination remains time-consuming and energy-intensive, accounting for more than 50% of the recycling cost. The regenerated graphite exhibits superior electrochemical performance, including high initial specific capacity (>350 mAh g^{-1}) and desired cycling stability (Table S1, Supporting Information) under a reasonable areal capacity (<0.7 mAh cm^{-2}).[12,15–25] When the areal capacity increases to ≈2.0 mAh cm^{-2}, the initial specific capacity and its retention become less promising.[3] Recent effort has shown that the performance gap between pristine graphite and regenerated graphite is attributed to the remaining surface and composition defects, which are common for spent anodes but fails to be addressed by direct calcination or wet chemistries.[3,18]

Typical failure of rechargeable LIBs is seen by the capacity fade of the cells and polarization buildup upon cycling. Previous research has revealed that there are several principal mechanisms for this failure,[21,26,27] including the loss of lithium inventory and active materials, impedance change, and stoichiometric drift, where the electrodes become imbalanced relative to each other. The capacity and power fade are mainly because of the irreversible loss of electrochemically active lithium and drastic changes in the electrode resistance, which are reflected in incremental polarization between Li insertion and deinsertion, and they are related to accumulation of the passivation layer.[28,29] The passivation layer includes insoluble Li organic and inorganic salts, which are reduction products that precipitate as surface films on the electrode. This constitutes the solid-electrolyte interphase (SEI), which is a Li-ion conductor but electronic insulator, passivating the surface and preventing detrimental electrode reactions. The Li inventory is consumed to form the SEI; this layer also traps other species dissolved in the electrolyte. Other factors, such as cathode metal ion (cobalt and nickel) dissolution and transfer,[27] delamination of active materials, mechanical stress-induced surface defects, and amorphization play roles in capacity decay.[5,29] These combined effects produce an insulating layer with a complex composition on top of the graphite particles, although the underlying crystalline graphitic structure is preserved and therefore worth recycling. Therefore, an effective anode recycling method should involve the SEI and binder removal, surface structure modification as well as the battery metals recollection with a high efficiency and a low environmental footprint.

Disclosed here is a flash recycling method that directly treats anode waste from spent LIBs while recovering valuable battery metal resources such as Li, Co, Ni, and Mn. This is done via a flash Joule heating process[30–33] within seconds and subsequent dilute acid (e.g., 0.1 M HCl) treatment (**Figure 1**a). The ultrafast electrothermal reaction heats the resistive layer with high selectivity, due to the Joule's law.[34] The pulsed current brings the anode waste to a temperature of ≈2850 K, leading to the decomposition of the SEI, polymer binder, and intercalated molecules together with the formation of a close-contact carbon coating, while retaining the graphite particle morphology. The estimated energy cost is ≈$118 to flash recycle 1 ton of untreated anode waste (Note S1, Supporting Information). Other decomposition products include simple inorganic salts such as LiF, and metal oxides such as Li_2O and CoO, which are easily recovered by the 0.1 M HCl treatment. The flash-recycled anode shows a recovered specific capacity of 351.0 mAh g^{-1} at 0.2 C, along with superior rate performance and electrochemical stability when compared to untreated anode waste and a calcination-recycled anode. The demonstration of full cells with two different cathodes, $LiFePO_4$ or NMC622 ($LiNi_{0.6}Mn_{0.2}Co_{0.2}O_2$), shows that the flash-recycled anode has an electrochemical stability and rate performance comparable to new graphite anodes. Life cycle analyses and comparisons to the graphite production and current calcination methods indicates that the flash recycling method for anode waste can significantly reduce the total energy, water consumption, and greenhouse gas emissions, underscoring the favorable environmental and economic impact using the flash recycling method.

2. Results and Discussion

2.1. Flash Recycling of Graphite Anodes

In a typical flash recycling process, the anode waste collected from spent LIBs is directly used as the reactant without further treatment. The powdered anode waste is slightly compressed inside a quartz tube between two graphite electrodes. The capacitor banks in the flash Joule heating circuit are used to provide electrothermal energy to the anode waste reactants for ≈1 s (Figure 1a and Figure S1, Supporting Information). Compared to the graphite particles, the SEI layer and other impurities are resistive. Therefore, the selective electrothermal effect can be achieved according to the Joule's law (Figure 1b), leading to the decomposition of these interfacial continuous phase resistive layers and the formation of simple inorganic salt and metal oxide nanoparticles. The flashed product is called flashed anode waste, including a close-contact carbon coating, along with the embedded nanoparticles, which are preserved during the ultrafast treatment. These simple inorganic compounds include battery metal resources, such as Li and Co, and they are highly soluble in 0.1 M HCl, increasing the overall efficiency of metal recovery. The flashed product after the dilute acid treatment is called flash-recycled anode. During the typical flash recycling process with a voltage of 120 V and a resistance of ≈1.3 Ω for the anode waste, the current passing through the sample reaches ≈350 A in ≈200 ms discharge time (Figure 1c) and the total amount of electrical energy is 12.1 kJ g^{-1}, corresponding to an average powder density of ≈48.4 kW g^{-1}. The temperature is measured using a high-temperature infrared thermometer with the maximum temperature ≈2850 K. The heating rate is ultrafast, at ≈1.6×10^5 K s^{-1} and the cooling rate is ≈9.2×10^3 K s^{-1} during the flash process (Figure 1d). A finite element simulation shows the homogeneous distribution of the momentary high temperature in the flash process (Figures S2 and S3, Supporting Information). The flash recycling process achieves the momentary and selective heating of the resistive layers; and the surrounding environment facilitates the subsequent rapid heat dissipation to avoid thermal expansion and defect formation of the graphite anode. In the traditional calcination

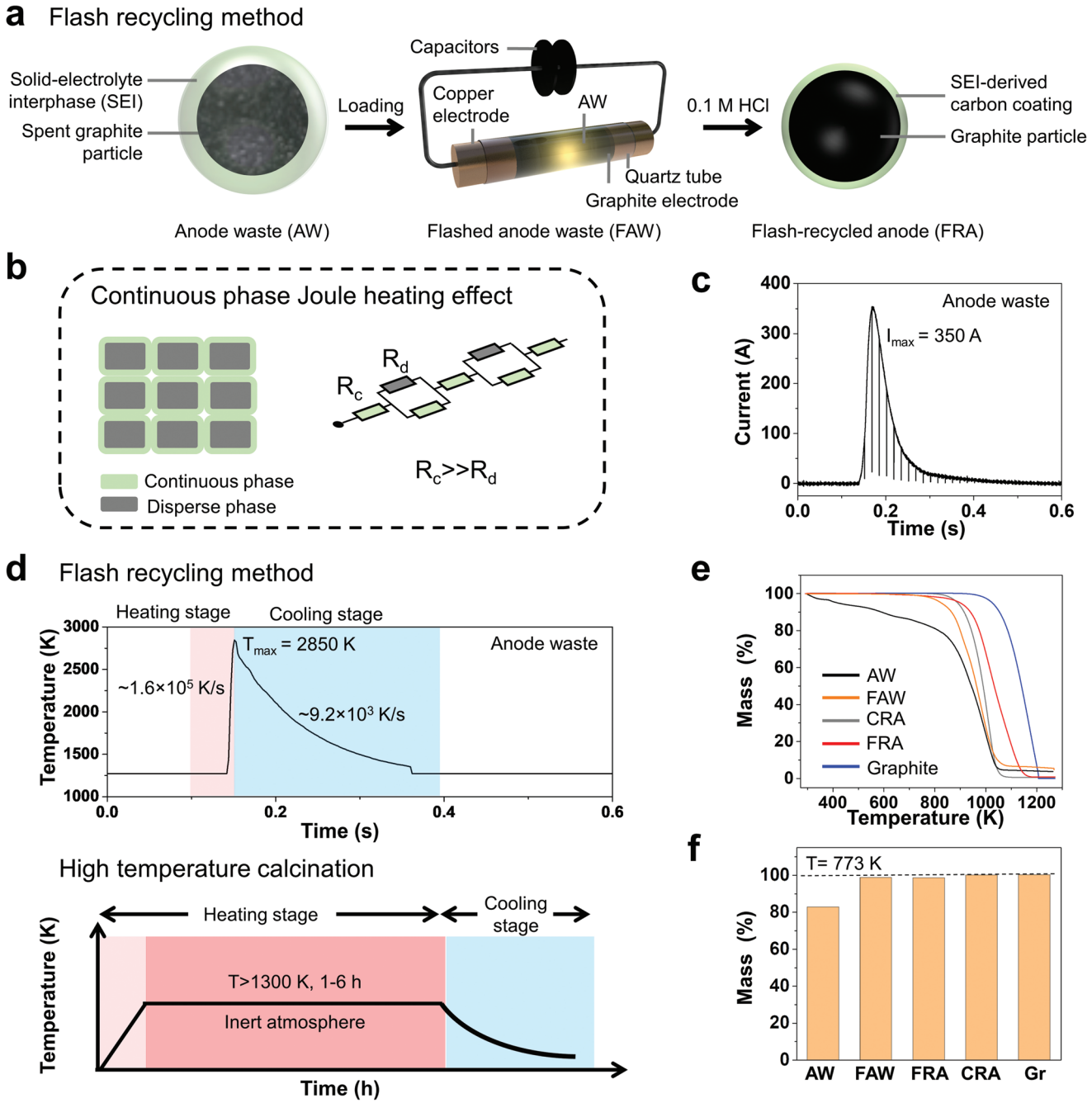

Figure 1. Flash recycling of graphite anodes. Schematic of a) flash recycling of AW and b) resistance-dependent Joule heating effects in multiple phase systems. c) Corresponding current-time curve during the flash recycling process. d) General procedures for flash recycling compared with conventional high temperature calcination and their real-time temperature curves. e) TGA thermogram of different graphite anodes. f) The remaining mass ratios of different graphite anodes at $T = 773$ K compared to the initial mass at 298 K. AW: anode waste. FAW: flashed anode waste. FRA: flash-recycled anode. CRA: calcination-recycled anode. Gr: graphite.

process, the entire system, including the furnace environment surrounding the anode waste, is subjected to high temperature (>1300 K) under an inert atmosphere to gasify all the impurities (Figure 1d), which consumes high energy, generates more greenhouse gas and leads to additional secondary waste.[3,35] The calcination-recycled anode shows larger surface area and more surface defects, contributing to the lower initial Coulombic efficiency (CE) and inferior stability than pristine anode materials, which will be discussed later. In addition, specific heat-resisting materials and heaters are required for a high-temperature calcination. These factors increase the capital and operation cost for traditional high-temperature calcination methods. Although prior work has reported that low temperature calcination (≈800 K for 2 h) can be used to remove most organic impurities, the

residue salts still require a 1.5 M HCl solution to achieve >99% recovery efficiency.[22] Recent work has shown that the rapid electrothermal method can be applied to evaporate the impurities, including the binder and SEI, especially the lithium salts LiF and Li_2CO_3.[17] Their results were similar to the traditional high-temperature treatment under inert atmosphere. The evaporation of the volatile compounds, and the expansion of the graphite structures were observed, leading to ≈40 times increasing of the surface area. However, the transition metal dissolution from the cathode and transfer to the anode is another common reason for performance decay for the commercial LIBs.[27] Since most transition metals have much higher boiling points (≈3200 K for Co and Ni), direct evaporation can be energy-intensive and causes the structure defects of the graphite microparticles (e.g., interlayer expansion, and sheet size reduction). In comparison, our flash recycling process involves the thermal decomposition of the hard-to-dissolve compact solid electrolyte interphase and binder, together with the collection of the battery metals from the flashed anode waste, demonstrating a more general strategy to regenerate the graphite anode and recollect the battery metals from the complex anode wastes in the spent LIBs.

To evaluate the removal of these resistive impurities in the flash recycling process, thermogravimetric analysis (TGA) is used since the thermal stabilities of the SEI, binder, graphite, and inorganic salts are distinct[36,37] (Figure 1e and Figure S4, Supporting Information). For untreated anode waste, there is ≈17.3 wt% mass loss at 773 K (Figure 1e), which includes the removal of the intercalated electrolyte, binder, and SEI layers. After the flash reaction, the mass loss decreases dramatically. The weight loss for flash-recycled anode is negligible at ≈1.4 wt%. A similar result is observed for calcination-recycled anode, which is prepared by calcination at 1323 K for 1 h under argon, with minimal mass loss of <0.1 wt% at 773 K. T_{50} reflects the temperature at which 50 wt% weight loss takes place,[38] which can be used to evaluate the thermal stability of the anode materials. T_{50} for flash-recycled anode is ≈1033 K, which is ≈90 and ≈50 K higher than in anode waste and calcination-recycled anode, which indicates the flash recycling method can improve the graphite stability. Gram-scale flash recycling is demonstrated (Figures S5 and S6, Supporting Information) and the input energy is 10.6 kJ g^{-1}. Therefore, the optimal electricity cost for flash step is ≈$118 ton^{-1} (Note S1, Supporting Information). Since the large-scale production of flash-recycled anode relies on not only the reactant mass in each batch, but also the ability to carry out the reaction in a continuous manner, we propose a design to achieve the continuous running of the FJH process as shown in Figure S7 and Note S1, Supporting Information.

2.2. Metal-Ion Leaching Tests on Anode Waste

The main components of the remaining solid at 1273 K are simple inorganic metal oxides (Figure S8, Supporting Information). For flashed anode waste, the remaining amount of inorganic oxides is ≈4.5 wt% (**Figure 2**a), and there is a slight increase of the relative ratio compared to the anode waste of ≈3.7 wt%, attributed to the removal of the other organic impurities. This ratio for calcination-recycled anode is ≈0.5 wt%, indicating the gasification and evaporation of most of the metal components. A previous study has pointed out that an ultrahigh temperature (>2800 K) is required to eliminate transition metals and their oxides due to their low vapor pressures.[5] Therefore, a subsequent acid treatment is often involved after high temperature treatment. To recover the valuable and toxic metal resources from flashed products, HCl solutions with different concentrations are used for comparison. Two factors, recovery efficiency (α) and excess yield (Y/Y_0) are defined to evaluate the recovery results (Note S2, Supporting Information). For one species (a metal from anode waste, flashed anode waste or calcination-recycled anode), α is the recovery yield obtained by a dilute acid relative to the recovery obtained from the raw anode waste using the concentrated 12 M HCl and Y/Y_0 is the yield obtained from various treated anode materials (flashed anode waste or calcination-recycled anode) relative to the yield obtained from untreated anode waste using the same acid recovery procedure.[39]

Figure 2b shows the absolute quantities of different metal components within the materials and compares the degrees of recovery and excess yields obtained under different recycling conditions and materials determined by inductively coupled plasma-optical emission spectrometry (ICP-OES). The total concentrations of Li, Co, and Ni reach 15 314 parts per million (ppm), 898 ppm and 124 ppm, respectively, in flashed anode waste, which are more concentrated than natural sources, such as ore and brine[40] (100–1000 ppm for Li) or seawater[41] (<0.21 ppm for Li). In addition, there is complex interference from other ions in natural sources such as seawater with Na^+ (≈13 000 ppm), Ca^{2+} (≈400 ppm), Mg^{2+} (≈2000 ppm), and K^+ (≈400 ppm). Conversely, previous work has shown that ≈100 ppm of the transition metal dissolution can be detrimental to battery stability, due to the accelerated electrolyte decomposition, and blocking of the Li^+ transfer through the SEI.[42] Therefore, complete collection of these battery metals cannot only achieve the critical metal sustainability, but also the regeneration of the graphite anode. The concentrations of these battery metal components are similar to anode waste, while they are ≈13 times higher than in calcination-recycled anode (Figure 2b). Direct high temperature calcination causes the evaporation of these metals, which condense downstream and might be corrosive to downstream equipment (Figure S9, Supporting Information). Thus, <15% of total metal ions can be collected at different aqueous HCl concentrations in calcination-recycled anode (Figure 2c). This result is consistent with the TGA results as shown in Figure 1e. Compared to 12 M HCl, dilute HCl (0.01–1 M) can effectively extract metal ions from the flashed anode waste; the average recovery efficiency reaches >99% using 0.1 M HCl (Figure 2d). The total amount of metal ions recovered from flashed anode waste is also higher than the recovery from untreated anode waste when using 0.1 M HCl, with an average excess yield of 1.11, which indicates 11% more metal ions can be collected from flashed anode waste. The improvement of leaching efficiency from flashed anode waste by using instead diluted acid (e.g., 0.1 M HCl) is attributed to the flash Joule heating treatment. The ultrafast electrothermal process raised the temperature to ≈2850 K, releasing battery metals from the complex organic matrix to produce simple inorganic compounds while reducing the metal compounds from their high valance states to their counterparts with lower valance states or metals[39] (Figure 2e and Table S2, Supporting

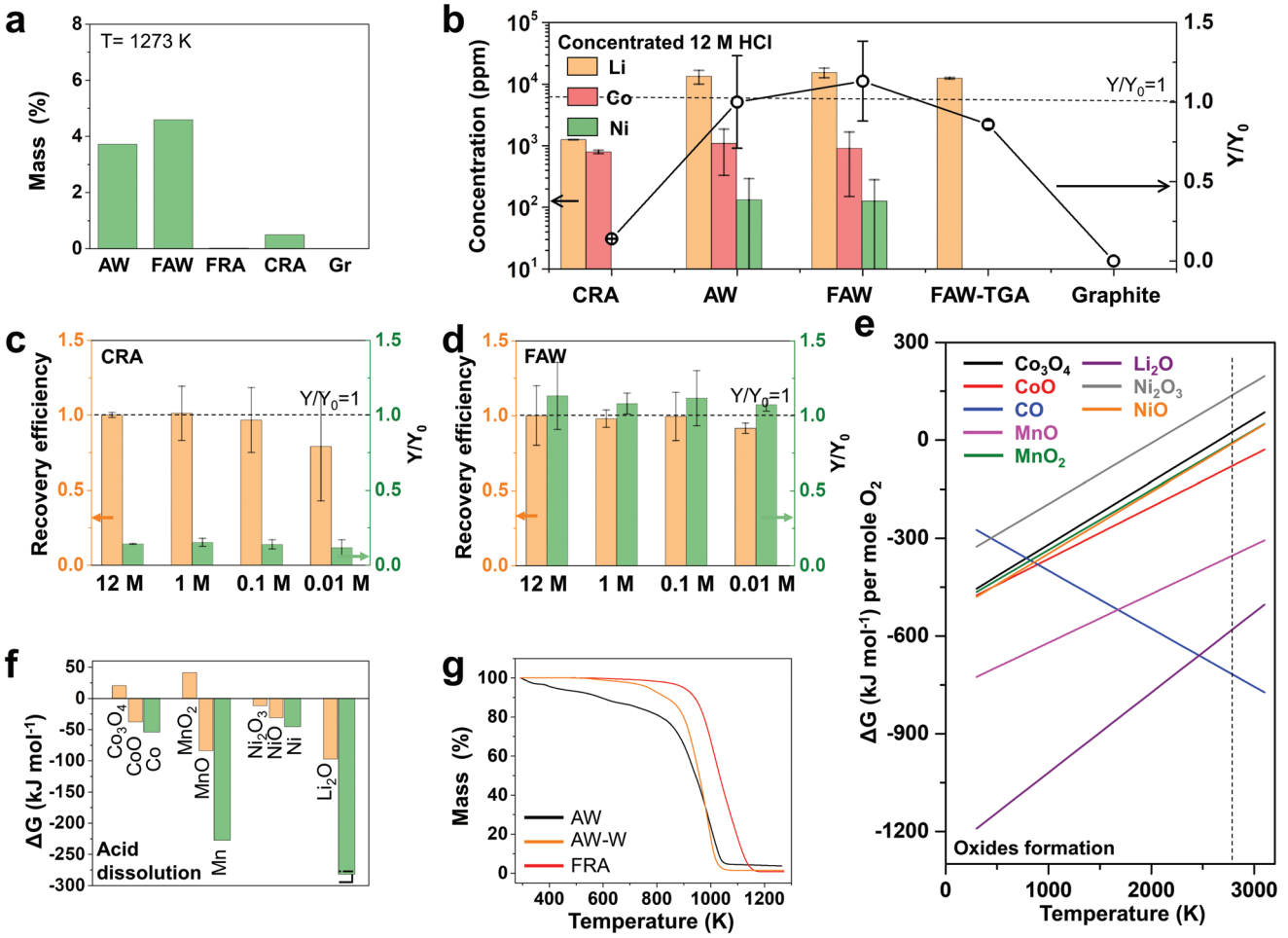

Figure 2. Metal-ion leaching tests on anode waste. a) The remaining mass ratios of different graphite anodes after calcination at $T = 1273$ K compared to the initial mass at 298 K. b) The total amounts of various metal ions and excess yields Y/Y_0 of total metal ions from different graphite anodes after treatment with concentrated 12 M HCl. The number of samples $N = 3$ and the bars show the standard derivations between runs, the same below. The dashed line denotes $Y/Y_0 = 1$, where Y_0 is the total metal ions from untreated anode waste and Y is the total metal ions from various graphite anodes. c) The recovery efficiency and excess yield Y/Y_0 of total metal ions for CRA by HCl treatment at different concentrations. d) The recovery efficiency and excess yield Y/Y_0 of total metal ions for FAW by HCl treatment at different concentrations. e) Ellingham diagram of carbon monoxide and various metal oxides. The dashed line denotes the flash temperature at 2850 K. f) Gibbs free energy change of the metal oxide and corresponding metal dissolution reactions in acid. g) TGA thermogram of different graphite anodes. AW: anode waste. AW-W: untreated anode waste after rinsing with 0.1 M HCl. CRA: calcination-recycled anode. FAW: flashed anode waste. FAW-TGA: flashed anode waste after TGA treatment. FRA: flash-recycled anode.

Information). This result is supported by the X-ray diffraction (XRD), high-resolution transmission electron microscopy (HR-TEM) and corresponding elemental mapping results, which shows the formation of the metal oxide nanoparticles, such as cobalt oxide and lithium oxide (Figures S10–S12, Supporting Information). Compared to the high valance state compounds, there are larger Gibbs free energy change (ΔG) values of the acid dissolution reactions for the metals and lower valance state counterparts (Figure 2f and Table S3, Supporting Information), indicating a higher thermodynamic solubility. The dissolution curves as a function of pH have also demonstrated that high valance state metal ions, like Co^{3+} only show slight solubility of ≈0.0075 mol L^{-1} when pH < 1, while Co^{2+}, Ni^{2+}, and Mn^{2+} remain soluble at >1 mol L^{-1} at a low pH ≈5 acidity.[7] Therefore, traditional hydrometallurgical methods always require a concentrated acid treatment[15,22] or an extra reductive reagent[11,20] to achieve high metal recovery yields. This can also explain the pH-dependent solubility of the untreated anode waste (Figure S13, Supporting Information) and excess yield of flashed anode waste when the dilute acid solutions are used (e.g., 0.1 M HCl). After rinsing flashed anode waste with 0.1 M HCl, the flash-recycled anode does not have appreciable solid (<0.1%) remaining at 1273 K (Figure 2g). This result is not achieved in our hands by rinsing the untreated anode waste with 0.1 M HCl (AW-W sample). The high resolution XRD spectrum shows that there are still many other diffraction peaks from the impurities (Figure S14, Supporting Information), including the lithium and transition metal salts. The TGA results are used to determine the remained mass ratios after the dilute acid treatment. There is still ≈5.3 wt% mass loss at 773 K and the remaining amount of inorganic residues is ≈1.4 wt% at 1273 K (Figure 2g), indicating the incomplete dissolution of the SEI and other

impurities with the direct dilute acid treatment. This is consistent with the acid leaching results as shown in Figure S13 (Supporting Information). The possible reason for the incomplete dissolution is that these crystals are embedded in the polymer matrix of the SEI, which hinders the acid dissolution and causes a low leaching efficiency. In conclusion, metal leaching tests demonstrate that anode waste from spent LIBs can be an alternative for collecting battery metals. The flash Joule heating reaction facilitates the acidic dissolution of these metals from anode waste, due to their release from complex organic matrix and the thermal reduction to low valance state counterparts.

2.3. Characterization of Flash-Recycled Graphite Anodes

To explore the changes after the flash recycling process, the bulk crystal structures of the products are analyzed by XRD. The crystal structures of the flash-recycled anode and anode waste are compared with commercial graphite in **Figure 3**a and Figure S15, Supporting Information. The graphitic structure is preserved for the untreated anode waste, while the accumulation of other inorganic salts, including LiF and Li_2CO_3, can be observed. After the flash Joule heating treatment, the (002) diffraction peak shows a small downshift to ≈26.5°, corresponding to the slight increase in the interlayer spacing of ≈0.3% over the commercial graphite (Figure S10, Supporting Information). This thermal expansion of the (002) spacing is also observed for calcination-recycled anode with the value of ≈0.2% (Figure S14, Supporting Information). The sharp (002) diffraction peak of flash-recycled anode is at ≈26.6°, which indicates the interlayer distance is ≈3.35 Å and matches that of a layered graphite structure (Table S4, Supporting Information).[37] The high-resolution spectra shows that there are no diffraction peaks from other species (Figure S15b, Supporting Information), which indicates that the flash recycling method is effective in purifying the graphite microparticles. The Raman spectra of untreated anode waste show the existence of obvious fluorescence bumps, other than the D, G, and 2D bands that can be observed in commercial graphite (Figure 3b and Figure S16, Supporting Information). These fluorescence bumps can be caused by the accumulation of the SEI layer on the surface of the graphite nanoparticles, and they disappear after the flash Joule heating treatment. The average Raman spectra are collected from 100 sampling points of the various graphite materials. The average D/G and 2D/G intensity ratios for flash-recycled anode are 0.14 and 0.56, respectively (Figure 3c), which reflects the defects and graphite quality, respectively.[34] They are similar to those values of commercial graphite ($I_D/I_G \approx 0.12$ and $I_{2D}/I_G \approx 0.57$). On the contrary, the calcination-recycled anode has a higher I_D/I_G of ≈0.29 and a lower I_{2D}/I_G of ≈0.44 (Table S4, Supporting Information). These results indicate that flash recycling method can be superior to preserving the bulk structure and graphite quality, together with avoiding the formation of extra defects.

X-ray photoelectron spectroscopy (XPS) can reflect the change of various elements and untreated anode waste is rich in C (41.8%), F (26.1%), metals (Li, Co, Mn, and Ni, 18.2%), O (12.9%), and P (1.9%) (Figure 3d and Table S5, Supporting Information). Deconvolution of the spectra reveal the existence of organic materials, metal fluoride and carbonate (Figure S17, Supporting Information), which are common components of the SEI layer.[43] The flash-recycled anode has a higher content of C (90.8%), and a decrease in the other elements (Figure S18, Supporting Information). Compared to the flashed anode waste (Figure S19, Supporting Information), the metal content of the flash-recycled anode is undetectable, which indicates the effective extraction of the metals by 0.1 M HCl leaching. This result is consistent with the ICP-OES analysis. calcination-recycled anode also has a high content of C (92.8%) and reduced content of other elements F (1.1%) and O (6.1%) at the surface (Figure S20, Supporting Information). The commercial graphite used for comparison shows C of 98.6% at the surface, which is slightly higher than that of calcination-recycled anode and flash-recycled anode (Figure S21, Supporting Information). The removal of the original organic SEI and electrolyte residue on untreated anode waste can be further confirmed by UV–vis spectra. After dispersing the untreated anode waste in deionized water, the supernatant is yellow in color and has a broad absorption peak centered at ≈220 nm (Figure 3e), which presumably results from the oxidized carbonate electrolyte and organic SEI.[44] In comparison, flash-recycled anode dispersed in water at the same concentration (≈5 mg mL^{-1}) produces a clear and colorless solution and there are no obvious absorption peaks for flash-recycled anode. A similar result is also observed for calcination-recycled anode dispersed in water at the same concentration (Figure S22, Supporting Information).

The bulk structures and morphologies of various graphite microparticles can be compared by scanning electron microscopy (SEM) as shown in Figure S23, Supporting Information. The particle size distributions are based on at least 50 different microparticles. There is no obvious change of the average particle sizes (≈15 µm) after the flash recycling process (Figure 3f). For untreated anode waste, the graphite microparticles are bound together by an organic binder (Figure 3g), while individual graphite microparticles are observed after the flash recycling process (Figure 3h). This result indicates the removal of the organic binder by the flash recycling method.

To pinpoint the change of surface structures, high resolution transmission electron microscopy (HR-TEM) is conducted. For anode waste (Figure 3i), there is an amorphous layer outside the graphite microparticles with an average thickness of ≈145 nm. The lattice fringes of graphite can be distinguished below this layer (Figure S24, Supporting Information). Within the amorphous layer, there are several embedded small Li_2CO_3 crystals, which agrees with the mosaic model of the SEI structure.[45,46] Scanning TEM (STEM) and the corresponding elemental distribution results show that metal elements are distributed homogeneously within the anode SEI for the untreated anode waste (Figure S25, Supporting Information). The existence of transition metals like Co (≈0.2 at%) within the SEI at the anode side is not unexpected. Cobalt dissolution from lithiated metal oxide cathodes has been observed in cells at the end of their lifespan.[27,47] Since SEI traps electrolyte, it could also trap dissolved transition metal ions. After the flash reaction, the SEI layer is thermally decomposed, the carbon portion is graphitized, and the average thickness shrinks to ≈40 nm for flashed anode waste (Figure S11, Supporting Information). Carbon shells with embedded nanoparticles, such as CoO, can

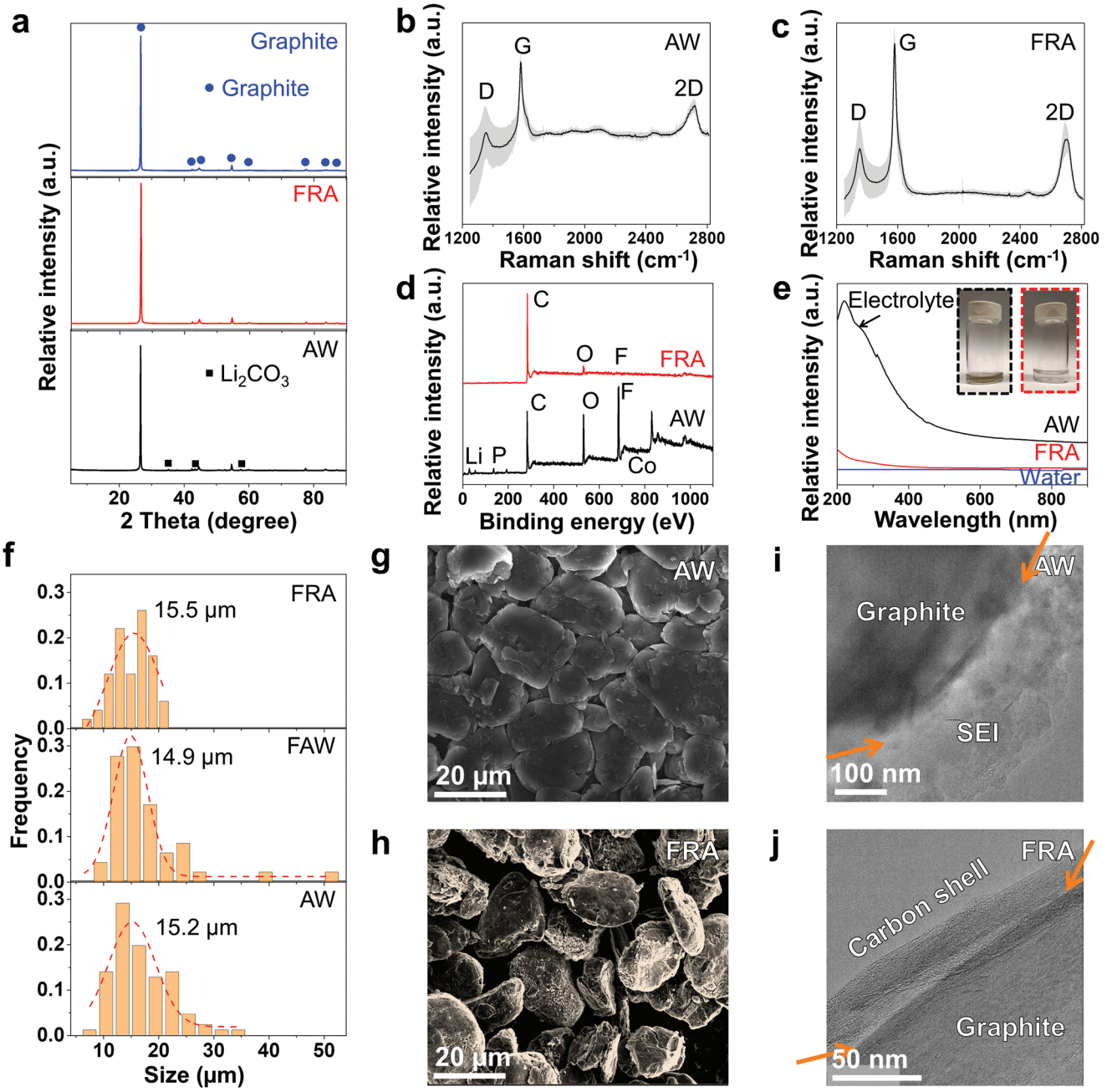

Figure 3. Characterization of flash-recycled graphite anodes. a) Crystal structures by XRD of commercial graphite (blue), FRA (red) and AW (black). Powder Diffraction File 89-8487, Graphite (circle). 01-0996, Li_2CO_3 (square). Statistical Raman spectra of b) AW and c) FRA. The black line and the gray shadow represent the average value and the standard deviation of 100 sampling points, respectively. d) Surface compositions by XPS of FRA (red) and AW (black). e) UV–vis spectra of the water leaching solution of FRA (red) and AW (black). The optical images show the yellowish solution and transparent solution derived from AW (black frame) and FRA (red frame), respectively. f) The SEM-determined size distributions of AW, FAW and FRA based on at least 50 different graphite particles. SEM images of g) AW and h) FRA microparticles. TEM images of i) AW and j) FRA microparticles. The yellow arrows delineate the boundaries of graphite particles. AW: anode waste. FAW: flashed anode waste. FRA: flash-recycled anode.

be discerned at the outermost regions[48,49] formed from the metal elements in the untreated anode waste SEI layer. This is confirmed by the STEM results as shown in Figure S12, Supporting Information. Although these metal nanoparticles appear to be trapped by the reformed carbon layer, they can be removed by rinsing the material with diluted acid 0.1 M HCl. This is far lower than the 3 M HCl concentration that is normally used in anode waste recycling.[14,15] Based on our work, valuable battery metals can be recovered from flashed anode waste by a simple acid post-treatment. For flash-recycled anode (Figure 3j), the carbon shell can be distinguished without metal nanoparticles, and the corresponding fast Fourier transform

(FFT) result reports one set of six-fold diffraction patterns along the [002] zone axis (Figure S26, Supporting Information), which reflects the preservation of well-graphitized anode particles.

2.4. The Electrochemical Performance of Flash-Recycled Anodes

To evaluate the effectiveness of the flash recycling method, the electrochemical properties of various anode materials, including the bulk resistivity, initial Coulombic efficiency (CE), rate performance and electrochemical stability, were tested. The polarization build-up during the charge and discharge process, caused by an accumulation of the SEI and surface amorphization, is one of the major reasons for anode failure.[3,5] As listed in Table S6 (Supporting Information), the pronounced ≈81% decrease of the bulk resistivity from anode waste to flash-recycled anode indicates the decomposition of resistive SEI, organic binder, and electrolyte residue. This result is similar to that found in the calcination-recycled anode, with ≈89% decrease of the bulk resistivity from the untreated anode waste. The skeletal density of the anode materials is ≈2.12 g cm^{-3} (Note S3 and Table S7, Supporting Information), which is consistent with the value reported in previous work.[50]

The voltage profiles of various anode materials at 0.05 C during the initial cycle are shown in **Figure 4**a. The areal capacities of the tested anodes are ≈2.0 mAh cm^{-2}. The charge specific capacity for the untreated anode waste is ≈269 mAh g^{-1}, which is ≈78 mAh g^{-1} smaller than that found in the flash-recycled anode. The reduction of solution components, including solvent and salt anions, and the simultaneous growth of the SEI happen at 0.5–1.5 V (vs Li/Li$^+$).[29] The capacity contribution for flash-recycled anode at this range is ≈43 mAh g^{-1}, which is smaller than the values of untreated anode waste (≈47 mAh g^{-1}) and calcination-recycled anode (≈56 mAh g^{-1}). This result is also

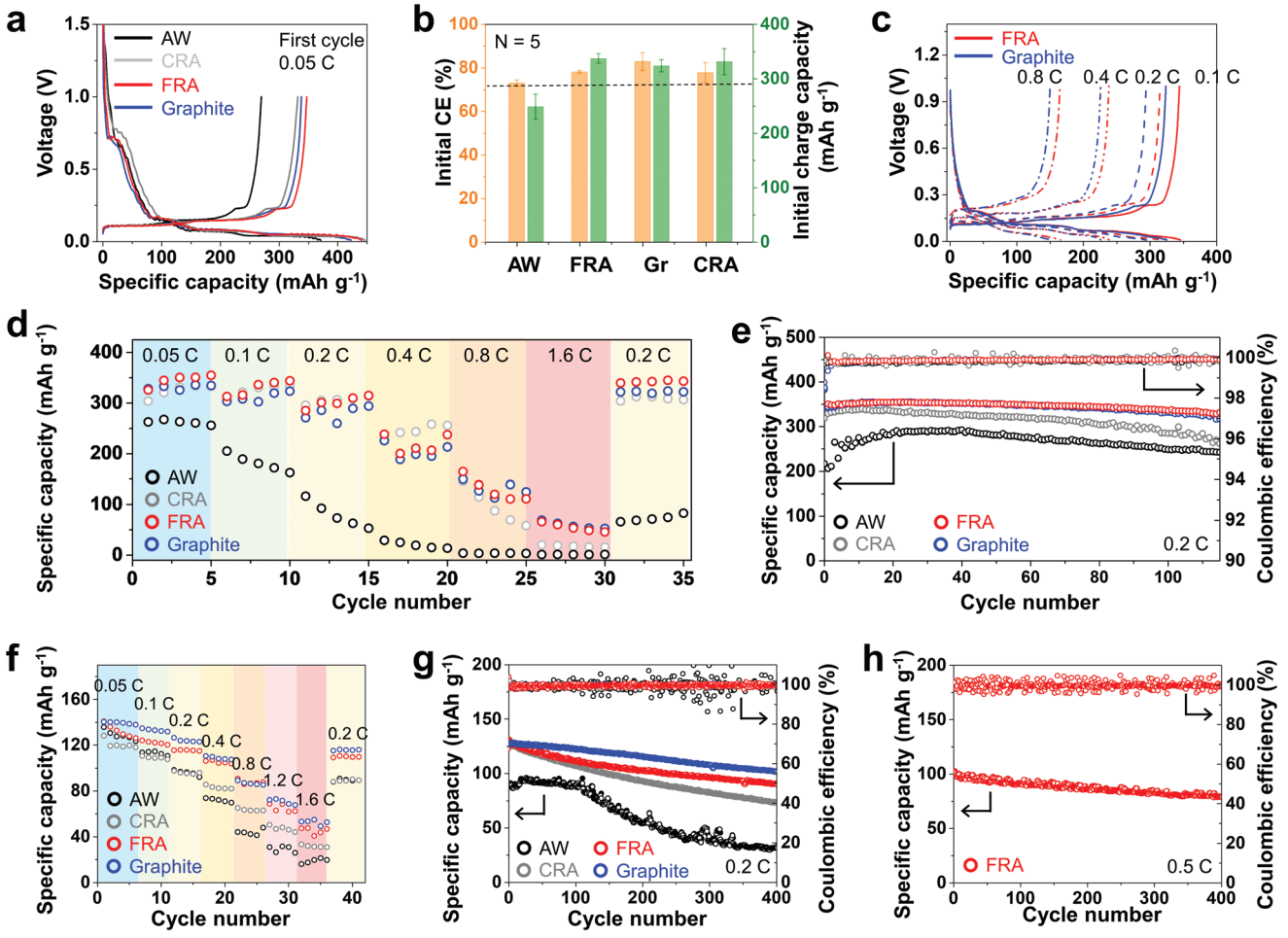

Figure 4. The electrochemical performance of flash-recycled anodes. a) First cycle voltage profile of AW (black), CRA (gray), FRA (red) and commercial graphite (blue) at 0.05 C. The areal capacity is ≈2.0 mAh cm^{-2}. b) The statistical results of initial CE and charge capacity of AW, FRA, commercial graphite, and CRA. The number of samples N = 5. The dashed line represents 80% of the designed capacity of graphite. c) Voltage profile of commercial graphite (blue) and FRA (red) at different rates. d) Rate performance of AW (black), CRA (gray), FRA (red), and commercial graphite (blue). e) Cycling performance of AW (black), CRA (gray), FRA (red), and commercial graphite (blue) at 0.2 C after operating at 0.05 C for 5 cycles. f) The rate performance of AW (black), CRA (gray), FRA (red), and commercial graphite (blue) with a$LiFePO_4$ cathode. g) Cycling performance of AW (black), CRA (gray), FRA (red), and commercial graphite (blue) with a $LiFePO_4$ cathode at 0.2 C. h) Cycling performance of FRA with a $LiFePO_4$ cathode at 0.5 C. AW: anode waste. CRA: calcination-recycled anode. FRA: flash-recycled anode. Gr: graphite.

very close to commercial graphite (≈37 mAh g^{-1}). The initial CE and charge specific capacities of at least 5 individual electrodes are measured for different anode materials. The average initial CE and charge specific capacities of flash-recycled anode are 78.1% and 336.9 mAh g^{-1}, respectively (Figure 4b), which shows obvious improvement compared to those of the untreated anode waste (72.9% and 248.3 mAh g^{-1}). These values are like those found in calcination-recycled anode (77.7% and 331.2 mAh g^{-1}), and they are comparable to commercial graphite (82.8% and 323.5 mAh g^{-1}). These initial charge specific capacities are slightly lower than the theoretical value of graphite (≈372 mAh g^{-1}), but they can be improved by the design of cycling protocols and the formation cycles (Note S4, Supporting Information).[51] The surface areas and pore size distributions of various anode materials are determined by N_2 adsorption/desorption curves as shown in Figures S27–S28, and Table S4, Supporting Information. The surface area of untreated anode waste is 9.0 m^2 g^{-1}, which is larger than the commercial graphite with surface area of ≈4.0 m^2 g^{-1} used in the work. The increases of the surface area are observed for both the calcination-recycled anode of ≈12.6 m^2 g^{-1} and flash-recycled anode of ≈15.4 m^2 g^{-1}, contributing to a slight larger initial specific capacity and a lower CE that those of commercial graphite.[17,18] However, the pore size distribution of the flash-recycled anode shows the domination of the micropores, with the pore size less than 2 nm. Since the typical sizes of the solvated PF_6^- and Li^+ reach up to 2 nm,[52,53] the slight larger surface area does not cause the severe reduction of the initial CE. Conversely, the direct use of the flashed anode waste or acid washed anode waste as the active materials still suffers from a lower specific capacity of ≈10%, and poorer stability and rate performance, when compared with the flash recycled anode, when they are cycled with an areal capacity of 2.0 mAh cm^{-2} (Figure S29, Supporting Information). The capacity retention of flashed anode waste is 89.9% after 100 cycles (Figure S29, Supporting Information). The inferior performance can be attributed to the existence of the embedded inorganic components, such as the metal oxides, as shown in Figures S11 and S12 (Supporting Information).[47]

The diffusion coefficient of Li^+ and quasi-equilibrium open circuit potential during the charging and discharging process can be calculated by galvanostatic intermittent titration technique (GITT), which measures the potential changes between the relaxation potentials and cycling potentials during each current pulse (Figure S30, Supporting Information).[54,55] The calculation of Li^+ diffusion coefficients can be seen in Note S5 and Figure S31 (Supporting Information). The average Li^+ diffusion coefficients of flash-recycled anode during the discharge and charge processes are 3.6×10^{-11} and 4.0×10^{-11} cm^2 s^{-1}, respectively, which is a 4-fold and 7-fold increase compared with the untreated anode waste (Table S6, Supporting Information). These results are close to those of calcination-recycled anode, and they are comparable to the commercial graphite. The improvement of the diffusion coefficients by flash recycling method indicates that Li^+ intercalation and de-intercalation kinetics have been recovered, which alleviates the cycling polarization and lowers the overpotential, especially at a larger rate (>0.5 C). The voltage profiles of various electrodes at different rates are shown in Figure 4c and Figure S32 (Supporting Information). The average specific capacity of flash-recycled anode is 345.3, 329.9, 218.6, and 129.1 mAh g^{-1} at rates of 0.05, 0.1, 0.4, and 0.8 C, respectively. This result shows the enhanced rate performance relative to untreated anode waste and it is comparable to the values of commercial graphite in our work and the rate performance of regenerated graphite in the previous literature[3] when cycling under similar current densities (Note S4, Supporting Information). Once the rate is back to 0.2 C, the flash-recycled anode has a capacity of 342.4 mAh g^{-1}. Although the specific capacity of calcination-recycled anode is similar to that found in flash-recycled anode and commercial graphite at low rates (<0.5 C), there is an obvious loss of specific capacity and increase of the overpotential at high rates for calcination-recycled anode (Figure 4d and Figure S32, Supporting Information). The cycling stability of various anode materials are compared as shown in Figure 4e. The flash-recycled anode can deliver a capacity of 351.0 mAh g^{-1} at 0.2 C and 335.9 mAh g^{-1} is retained after 100 cycles, which is close to the electrochemical stability of commercial graphite. However, the calcination-recycled anode suffers from a faster decay (≈17%) after 100 cycles. Therefore, flash-recycled anode is more stable than calcination-recycled anode during the electrochemical cycling, which is attributed to the stability of the bulk structure and the graphene shell formed at the surface of flash-recycled anode by the flash recycling process (Figures 1e and 3), acting as the protecting layer and artificial SEI. The electrochemical performance of the flash-recycled anode prepared from gram-scale trials is also tested as shown in Figure S33 (Supporting Information), which demonstrates the similar improvement compared to the untreated anode waste.

The full battery tests are carried out with the $LiFePO_4$ as the cathodes. An improvement of the rate performance for flash-recycled anode is observed (Figure 4f), which is consistent with the above half-cell tests. There is a low specific capacity of ≈94.9 mAh g^{-1} and poor stability for the untreated anode waste, with the average capacity decay of 0.17% per cycle at 0.2 C for 400 cycles (Figure 4g). The specific capacities for flash-recycled anode and calcination-recycled anode are 131.1 and 129.8 mAh g^{-1}, respectively. However, flash-recycled anode has a better electrochemical stability with the decay of 0.078% per cycle (Figure 4g). The decay values for calcination-recycled anode and commercial graphite are 0.11% and 0.055% per cycle, respectively. The capacity retention of flash-recycled anode after cycling at 0.5 C for 400 cycles is ≈77.3% (Figure 4h), which shows good stability. The other commercial cathode, NMC622, has also been tested and the voltage profiles at 0.2 C are shown in Figure S34 (Supporting Information). Therefore, flash-recycled anode is compatible with different cathode materials after the flash recycling process.

2.5. Economic and Environmental Analysis of Flash Recycling Process

GREET 2020[56] and Everbatt 2020,[57] software developed by Argonne National Laboratory, are used to reflect the prospective cradle-to-gate LCA, which considers the economic and environmental impacts from the mining or preparation of reactants (cradle) to all reaction processes involving the production of 1 kg battery-grade graphite at the factory (gate). A cradle-to-gate LCA does not consider the use of the graphite products nor their disposal (grave) since it is assumed that

new graphite and recycled graphite have the same usage and recycling stages.[58,59] Four methods are compared in this section, including 1) synthetic graphite prepared from hard coal and crude oil,[60] 2) calcination-recycled anode prepared from high temperature calcination method,[13] 3) flash-recycled anode from the flash recycling method as described here, and 4) natural graphite from mined ore.[61] The process flow diagrams are shown in **Figure 5**a–c and Figure S35 (Supporting Informa-

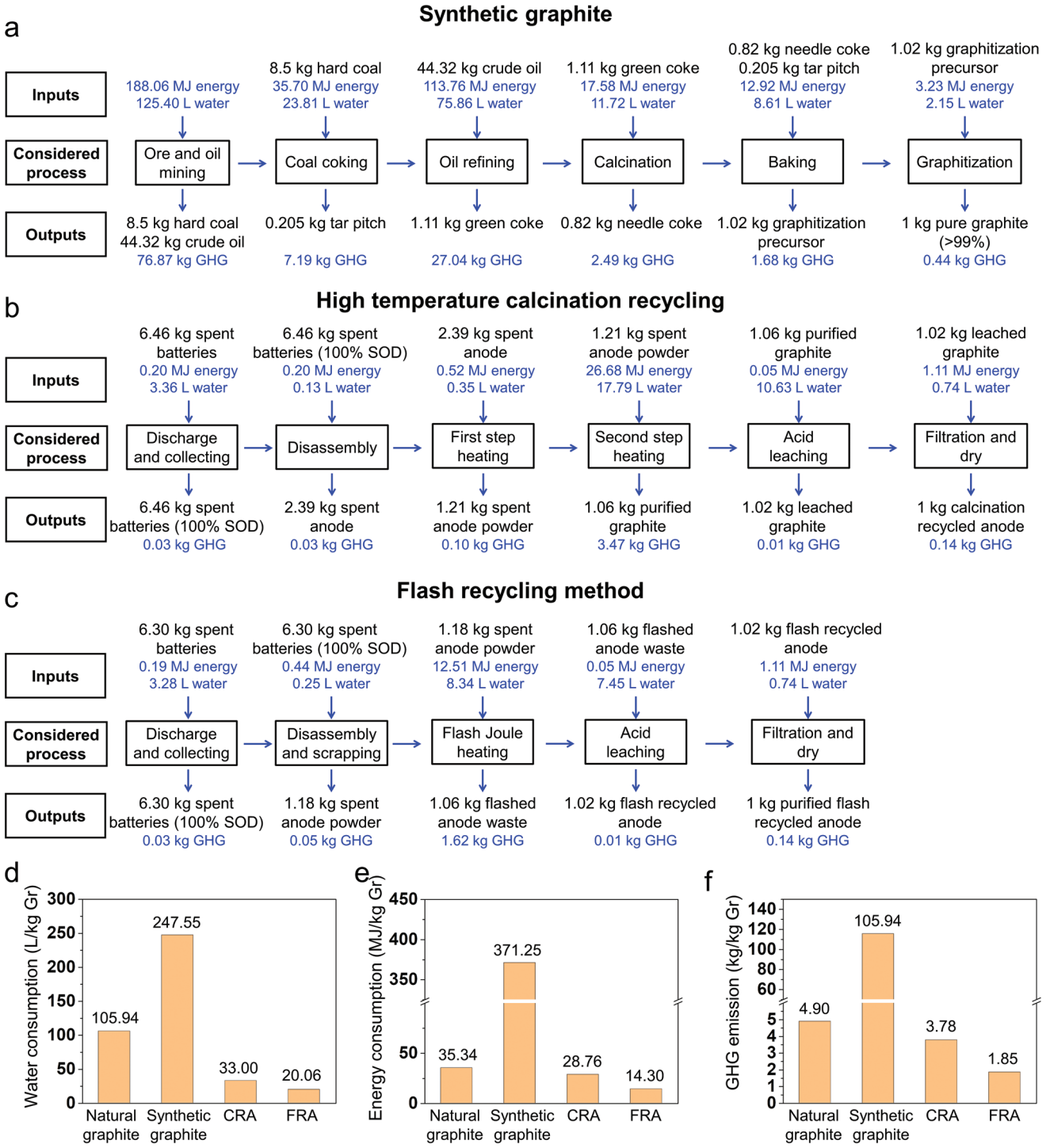

Figure 5. Economic and environmental analysis of the flash recycling process. a–c) Process flow diagrams of various battery-grade graphite production routes, displaying the lifecycle inventory including all considered inputs and outputs. Incidental inputs and outputs are shown in blue font to differentiate them from explicit inputs and outputs. a) Synthetic graphite production. b) High temperature calcination recycling. c) Flash recycling method. d) The water consumption, e) energy consumption, and f) greenhouse gas emission (GHG) in producing 1 kg of graphite anode materials. CRA: calcination-recycled anode. FRA: flash-recycled anode.

tion), and they are discussed in Note S6 (Supporting Information). A cut-off approach is employed in the case of the spent battery used in the high temperature calcination and flash recycling method. Therefore, the environmental impacts of the spent battery are associated with the prior product, and they are considered as battery waste without associated burdens. In addition, it is assumed that the use and end-of-life phases for the battery-grade graphite is identical regardless of the production pathway.[59] Thus, the cradle-to-gate LCA is used to study different production processes.

The detailed parameters regarding the inputs and outputs of each individual step for the above four methods are listed in Table S8 (Supporting Information). The results of cradle-to-gate LCA reflect that the flash recycling method results in substantial reductions in water and energy consumption, as well as the greenhouse gas emission when compared to the graphite production method and high temperature calcination recycling method (Figure 5d–f). Compared to the synthetic graphite production method, the flash recycling method reduces recycling cost by ≈85% (Figure S36, Supporting Information), greenhouse gas emissions by ≈98%, water use by ≈92%, and energy use by ≈96%. The large decrease is attributed to the elimination of the mining, refining and calcination steps, which accounts for ≈80% of the energy and water consumption for the synthetic graphite production method. Similar improvements are observed when comparing the flash recycling method to the natural graphite production method. The flash recycling method is shown to reduce the greenhouse gas emissions by ≈62%, water use by ≈81%, and energy use by ≈60%. The flash recycling method affords a 51% reduction in greenhouse gas, 39% decrease in water and 50% reduction in energy compared with high temperature calcination recycling method. The large reduction in energy for flash recycling method is mainly attributed to the adoption of the ultrafast electrothermal method to directly raise the temperature of the graphite materials to ≈2850 K in <1 s, which can decompose and remove the resistive impurities accumulated on the spent anode materials. In addition, the high energy efficiency due to the Joule's law [62] further highlights the advantage of using the flash recycling method.

3. Conclusion

In conclusion, we developed an ultrafast flash recycling method to recycle graphite anodes from untreated anode waste. The Joule heating effect causes the thermal decomposition of the resistive SEI and simultaneous formation of a carbon shell around the graphite microparticles. The intrinsic 3D layered graphite core structure is preserved. The metals Li, Co, Ni, and Mn can be easily recovered from the flash anode products by post-treatment with 0.1 M HCl. The flash-recycled anode shows a recovered specific capacity of 351.0 mAh g^{-1} at 0.2 C and a good electrochemical stability. The capacity retention is 77.3% after 400 cycles at 0.5 C when coupled with a $LiFePO_4$ cathode. A gram-scale production has been demonstrated. Since the flash Joule heating method is being industrially scaled up to 1 ton per day by early 2023 and targeted for 100 tons per day by 2024,[63] flash recycling has the potential to address the daunting accumulation of spent LIBs. At the same time, the flash recycling method affords a greener and more profitable approach to anode waste recycling.

4. Experimental Section

Materials: The mesocarbon microbeads (MCMB) graphite powder for Li-ion battery anode (19.0–23.0 µm, ≥99.50%, 0012106-250G) was purchased from MTI Corporation. Spent commercial lithium batteries (LG Chem 112711, B052R785-9005A) were obtained from used Lenovo laptop computers. Quartz tubing (ID = 8 mm, L = 6 cm) was used as the reactant FJH tube for small batches (200 mg per batch) and quartz tube (ID = 16 mm, L = 6 cm) was used for larger batches (1 g per batch) in the experiments. The standard solutions for inductively coupled plasma-optical emission spectrometry (ICP-OES) tests included cobalt standard (1000 ± 2 mg L^{-1}, 30329-100ML-F), lithium standard (998 ± 4 mg L^{-1}, 12292-100ML), manganese standard (1003 ± 5 mg L^{-1}, 74128-100ML), and nickel standard (998 ± 4 mg L^{-1}, 28944-100ML-F), all of which were purchased from Millipore-Sigma. The nitric acid (HNO_3, trace metal grade, 1120060) was purchased from Fisher Chemical and hydrochloric acid (HCl, 99.999% trace metals basis, 339253-100ML) was purchased from Millipore-Sigma. Water (HPLC Plus, 34877-4L) was purchased from Millipore-Sigma. *N*-methyl pyrrolidone (NMP, >99.0%, 443778-500ML) was purchased from Millipore-Sigma. Polyvinylidene fluoride binder (PVDF, 121120-80G) was purchased from MTI Corporation. High conductive acetylene black (ABHC-01, 342431) was purchased from Soltex Corporation. The milling ball (Yttrium stabilized ZrO_2, 99.5%, R = 5 ± 0.3 mm) was purchased from MTI Corporation. The 1 mol L^{-1} $LiPF_6$ in a mixture of ethylene carbonate (EC), diethyl carbonate (DEC) and dimethyl carbonate (DMC) (V:V:V = 1:1:1) electrolyte (battery grade, 901685-100ML) was purchased from Millipore-Sigma. Lithium iron phosphate ($LiFePO_4$, battery grade, 0011512) was purchased from MTI Corporation. NMC622 ($LiNi_{0.6}Mn_{0.2}Co_{0.2}O_2$, 2.0 mAh cm^{-2}, BE-54E) was purchased from NEI Corporation. Lithium chip (D = 16 mm, t = 0.6 mm, 99.9% Li) was purchased from MTI Corporation.

Characterization: TGA was performed on a Mettler Toledo TGA/DSC 3+ system. TGA and DSC data were collected at a heating rate of 10 °C min^{-1} under air. The air flow was set to 80 mL min^{-1}. XRD measurements were done by a Rigaku SmartLab Intelligent XRD system with filtered Cu Kα radiation (λ = 1.5406 Å). XPS data were collected with a PHI Quantera SXM Scanning X-ray Microprobe with a base pressure of 5×10^{-9} Torr. Survey spectra were recorded using 0.5 eV step sizes with a pass energy of 140 eV. Elemental spectra were recorded using 0.1 eV step sizes with a pass energy of 26 eV. All the XPS spectra were corrected using the C 1s peaks (284.8 eV) as reference. For the depth analysis, an Ar^+ ion sputtering source was used to etch the surface layer. The average etching rate was calibrated and was ≈7 nm min^{-1} in the experiment, which can be further used to estimate the depth. UV–vis (Shimazu UV-3600 plus) was used to collect the spectra of the suspension of reactant and flash products. The reactant and flash products were characterized through SEM using a FEI Helios NanoLab 660 DualBeam SEM at 5 kV with a working distance of 4 mm. TEM images and SAED patterns were taken with a JEOL 2100F field emission gun transmission electron microscope at 200 kV. HR-TEM and STEM images were taken with FEI Titan Themis S/TEM instrument at 300 keV after accurate spherical aberration correction. The metal contents in the reactant and flash products were quantified using a PerkinElmer Optima 8300 ICP-OES system. The samples were diluted with a 2% aqueous nitric acid solution, and calibration curves were generated using 7 ICP standard solutions (blank solution, 1, 2, 5, 10, 25, and 50 ppm standards), with the results used only from correlation coefficients that were greater than 0.999. The gas nebulizer flow rate range was set between 0.45 and 0.75 L min^{-1}, and 2 wavelengths per element were used in the axial mode unless otherwise stated: cobalt (228.616 and 230.786 nm), lithium (670.784 nm – radial mode – and 610.362 nm), nickel (231.604 and 341.476 nm), and manganese (257.610 and 259.372 nm). Raman spectra were collected with a Renishaw Raman microscope using a 532 nm laser with a power

of 5 mW. A 50 × lens was used for local Raman spectra. The statistical Raman spectra were obtained by mapping 100 evenly spaced locations in a 100 × 100 µm grid.

The bulk resistivities were measured from compact pellets prepared from individual powders. The sample powder was cold pressed to form a compact pellet before the resistance measurement. The diameter of the pellet was 16 mm, and the thickness of the pellet was measured by a micrometer. The loading pressure was ≈1000 psi. The pellet was compressed by two spacers (graphite and copper, Figure 1) at both sides and the resistance was measured by a high-resolution ohmmeter. Then the resistivity was calculated by the equation $\rho = \frac{R\pi r^2}{t}$. Here, R was the measured resistance, r was the radius, and t was the thickness of the pellet. The resistivity at 100% stacking density (ρ_0) was further estimated by the equation $\rho_0 = \frac{\rho}{0.74}$.[64]

FJH system: The FJH system has been described in the previous publications.[21,22] The circuit diagram and FJH reaction box are shown in Figure S1 (Supporting Information). Ar gas (≈1 atm) was used as an inert atmosphere to avoid sample oxidation during the FJH reaction. The reactant was the graphite anode waste collected from the anode side of the spent Li-ion batteries. The reactant powder was ground and mixed homogeneously by a mortar and pestle before being loaded to the reaction tube with an inner diameter of 8 or 16 mm. Here, the reaction tube can be a quartz or ceramic tube. The mass loads in the 8-mm and 16-mm tube were 200 mg and 1 g, respectively. Graphite rods are used as electrodes in this reaction. The compressing force was controlled by a small vise connected to a rotary knob as shown in Figure S1b (Supporting Information), to tune the sample resistance to ≈2 Ω. The Arduino controller relay with programmable millisecond-level delay time was used to control the discharge time and the electric energy was provided by a capacitor bank with a total capacitance of 60–222 mF. The capacitor bank was charged by a d.c. power supply capable of reaching 400 V. The FJH reaction was carried out with voltage 120 V and optimized duration of 1000 ms for 8-mm tube reaction. (More details are shown in **Table 1**.) After the FJH reaction, the apparatus was allowed to cool and vent for 3 min. The product was called flashed anode waste in this context. Additional safety notes can be seen in the Supplemental text.

Metal-Ion Leaching Tests: The metal-ion leaching tests were carried out for different anode materials, including anode waste, flashed anode waste, calcination-recycled anode and commercial graphite. calcination-recycled anode is prepared by calcination at 1323 K for 1 h under argon. HCl solution with different concentrations from 0.01 to 12 M were used. The anode samples (≈10 mg) were digested at 60 °C for 3 h. For all the tests, the molar ratios of the total H^+ in the acid solutions to metal-ions from anode samples were ≈10. Therefore, the fluctuation of the pH was negligible. The sample was then filtered using a PES membrane filter (0.22 µm) and diluted to 20 mL using ultrapure water for ICP-OES measurement.

Table 1. Flash parameter for different systems.

	Small batch	Large batch	Large batch (VFD)
Reactant	Graphite anode waste	Graphite anode waste	Graphite anode waste
Sample mass	200 mg	1 g	1 g
Sample resistance	≈1.3 Ω	≈1.0 Ω	≈1.4 Ω
Discharge voltage	120 V	164 V	140 V
Flash duration	1000 ms	1000 ms	VFD[a)]
Total capacitance	168 mF	222 mF[b)]	624 mF
Flash time	2	3	2
Chamber pressure		Ar or N_2 (≈1 atm)	

[a)]VFD is a type of controller that drives an electric switch by varying the frequencies and durations of its power supply. Here, 10% duty cycle for 1s followed by 25% duty cycle for 4 s was used. [b)]This is the nominal capacitance. The measured capacitance has decreased to ~205 mF after frequent usage of the capacitors for ~4 years.

Electrochemical Tests: All of the anodes (areal capacity ≈2.0 mAh cm^{-2}) were used for the half-cell test. The anode was prepared by grinding the mixture of anode materials, conductive carbon black and PVDF at a ratio of 0.8:0.1:0.1. A small amount (≈3.5 × of the total mass) of NMP was used to form a homogeneous slurry. The slurries were formed by ball milling at 1300 rpm for 30 min. The anode current collector was Cu/C foil with a thickness of 10 µm. The slurry was applied to the Cu/C foil by a doctor blade with blade spacing of 180 µm (≈1.2 mAh cm^{-2}) and 300 µm (≈2.0 mAh cm^{-2}). The electrode was dried using a built-in heating cover placed on top of the electrode at 70 °C for 2 h and then put in a vacuum oven overnight. The temperature and pressure of the vacuum oven were set at 70 °C and ≈10 mmHg. The area of the electrode was ≈1.54 cm^2. The electrolyte used was 1 M $LiPF_6$ in a mixture of EC, DEC, and DMC (*V*:*V*:*V* = 1:1:1). The volume of the electrolyte in each coin cell was 75 µL. Before the electrochemical test, the cells were pretreated at 0.05 C between 0.01 and 1.0 V for 5 cycles. Subsequently, the cells were galvanostatically cycled between 0.01 and 1.0 V at 0.2 C for stability tests. The anode waste collected directly from the spent batteries was used as the control sample. For the new graphite anode materials, the mixture ratio of new graphite, PVDF and conductive carbon black was 0.8:0.1:0.1. All the other operations were the same. The magnified discharge profiles in Figure S37 (Supporting Information) showed that the cut-off voltage was 0.01 V.

The $LiFePO_4$ cathode (areal capacity ≈1.0 mAh cm^{-2}, N/P ratio = ≈1.2) was used for the full cell tests. The cathode was prepared by grinding the mixture of $LiFePO_4$, acetylene black, and PVDF at a ratio of 0.90:0.05:0.05. A small amount (2.5 times of the solid weight) of NMP was used to form a homogeneous slurry. Slurries were formed by ball milling at 1500 rpm for 10 min. The cathode current collector was Al/C foil with a thickness of 18 µm. The slurry was applied to the Al/C foil by a doctor blade with blade spacing of 250 µm. The electrode was dried at 70 °C for 2 h and then put in a vacuum oven overnight. The temperature and pressure of the vacuum oven were set at 70 °C and ≈10 mmHg. The areas of the cathode and anode were ≈1.54 and ≈2.00 cm^2, respectively. The electrolyte used was 1 M $LiPF_6$ in a mixture of EC, DEC, and DMC (*V*:*V*:*V* = 1:1:1). The volume of the electrolyte in each coin cell was 50 µL. Before the electrochemical test, the cells were pretreated at 0.05 C between 3.0 and 3.8 V for 5 cycles. Subsequently, the cells were galvanostatically cycled between 3.0 and 3.8 V at 0.2 C or 0.5 C for stability tests.

Finite Element Simulation: Wolfram Mathematica 11.3[65] was used for preliminary data processing. To obtain a representative current versus time curve, current data from five separate flash reactions collected at 20 kHz were averaged together. To remove some spurious spikes resulting from measurement noise, a median filter of 10 adjacent datapoints was applied. Subsequently, a polynomial fit was performed, to represent the current flow in analytical form for ease of implementation. Using the parameters of the system, the voltage versus time, along with the time-dependent impedance of the sample were computed, to ensure that both charge and electrical energy conservation are maintained throughout the simulation.

The 2D-axisymmetric simulation was performed using COMSOL Multiphysics 5.5.[66] The properties of the system along with materials of interest[67,68] were defined as parameters within the model. An image of the mesh is included in Figure S3 (Supporting Information). The default mesh was not used, given that to resolve the transport processes it was necessary to further refine the mesh within the sample, which is the primary region of interest, along with the interfaces, where the predominant transport processes are occurring. A sufficiently dense grid mesh comprised of 13 750 domain elements and 990 boundary elements was chosen to be employed.

During the data workup process performed in Mathematica, it was found that the charge stored on the capacitors is depleted during the course of the reaction. After 0.23257 s, current becomes undetectable since the voltage rapidly approaches zero during the discharge process. Therefore, electrothermal heating was applied through specifying the

voltage on the terminal for the first 0.23257 s, after which the terminal was set to ground ($V = 0$). The finite element calculation was carried out using time steps of 0.0005 s, which was sufficiently small to resolve the transient processes that occur during the heating stage. Subsequently, the cooling stage ensued, during which the same time step was used. In total, the simulation was performed for three simulation seconds. The simulated temperature distribution along with a temperature contour plot at $t = 0.0745$ s is included in Figure S2 (Supporting Information), and a video of the arrangement of the components used during the flash process, along with simulated temperature distributions that occur during the heating and cooling process, is included in Video S1 (Supporting Information).

Statistical Analysis: The electrochemical data, ICP-OES results, and UV–vis results were used without any preprocessing. The XPS data, Raman results, TGA and XRD results were normalized based on the maximum intensity of the spectra for the purpose of presentation. The Raman results reflected the statistical analyses, in which the black line and the gray shadow represented the average value and the standard deviation of 100 sampling points, respectively. The size distributions of graphite anode samples were calculated from at least 50 particles.

Supporting Information

Supporting Information is available from the Wiley Online Library or from the author.

Acknowledgements

The funding of the research was provided by Air Force Office of Scientific Research (FA9550-22-1-0526) and the DOE-NETL (DE-FE0031794). The characterization equipment used in this project was from the Shared Equipment Authority (SEA) at Rice University. The authors acknowledge the use of the Electron Microscopy Center (EMC) at Rice University. The authors thank Dr. Bo Chen for helpful discussion of the XPS results, and Dr. Chris Pennington for method development of the ICP-OES tests. The authors thank the Earth, Environmental & Planetary Sciences Department, Dr. Yueyang Jiang, and Dr. Helge Gonnermann for graciously providing the access to COMSOL Multiphysics.

Conflict of Interest

Rice University owns intellectual property on the flash recycling process disclosed here. The authors claim no other conflicts of interest.

Data Availability Statement

The data that support the findings of this study are available from the corresponding author upon reasonable request.

Keywords

anode waste, flash recycling, graphite, life cycle analysis, lithium-ion batteries

Received: August 10, 2022
Revised: November 16, 2022
Published online: December 20, 2022

[1] R. V. Salvatierra, A.-R. O. Raji, S.-K. Lee, Y. Ji, L. Li, J. M. Tour, *Adv. Energy Mater.* **2016**, *6*, 1600918.
[2] M. Li, J. Lu, Z. Chen, K. Amine, *Adv. Mater.* **2018**, *30*, 1800561.
[3] B. Markey, M. Zhang, I. Robb, P. Xu, H. Gao, D. Zhang, J. Holoubek, D. Xia, Y. Zhao, J. Guo, M. Cai, Y. S. Meng, Z. Chen, *J. Electrochem. Soc.* **2020**, *167*, 160511.
[4] R. V. Salvatierra, W. Chen, J. M. Tour, *Adv. Energy Sustainable Res.* **2021**, *2*, 2000110.
[5] S. Natarajan, V. Aravindan, *Adv. Energy Mater.* **2020**, *10*, 2002238.
[6] Y. Zhao, X. Yuan, L. Jiang, J. Wen, H. Wang, R. Guan, J. Zhang, G. Zeng, *Chem. Eng. J.* **2020**, *383*, 123089.
[7] W. Lv, Z. Wang, H. Cao, Y. Sun, Y. Zhang, Z. Sun, *ACS Sustainable Chem. Eng.* **2018**, *6*, 1504.
[8] X. Hu, E. Mousa, Y. Tian, G. Ye, *J. Power Sources* **2021**, *483*, 228936.
[9] L. Li, E. Fan, Y. Guan, X. Zhang, Q. Xue, L. Wei, F. Wu, R. Chen, *ACS Sustainable Chem. Eng.* **2017**, *5*, 5224.
[10] Y. He, T. Zhang, F. Wang, G. Zhang, W. Zhang, J. Wang, *J. Clean Prod.* **2017**, *143*, 319.
[11] X. Ma, M. Chen, B. Chen, Z. Meng, Y. Wang, *ACS Sustainable Chem. Eng.* **2019**, *7*, 19732.
[12] Y. Gao, C. Wang, J. Zhang, Q. Jing, B. Ma, Y. Chen, W. Zhang, *ACS Sustainable Chem. Eng.* **2020**, *8*, 9447.
[13] I. Rey, C. Vallejo, G. Santiago, M. Iturrondobeitia, E. Lizundia, *ACS Sustainable Chem. Eng.* **2021**, *9*, 14488.
[14] Y. Guo, F. Li, H. Zhu, G. Li, J. Huang, W. He, *Waste Manage.* **2016**, *51*, 227.
[15] K. Liu, S. Yang, L. Luo, Q. Pan, P. Zhang, Y. Huang, F. Zheng, H. Wang, Q. Li, *Electrochim. Acta* **2020**, *356*, 136856.
[16] S. Rothermel, M. Evertz, J. Kasnatscheew, X. Qi, M. Gretzke, M. Winter, S. Nowak, *ChemSusChem* **2016**, *9*, 3473.
[17] S. Dong, Y. Song, K. Ye, J. Yan, G. Wang, K. Zhu, D. Cao, *EcoMat* **2022**, e12212.
[18] J. Luo, J. Zhang, Z. Guo, Z. Liu, S. Dou, W.-D. Liu, Y. Chen, W. Hu, *Nano Res.* **2022**, https://doi.org/10.1007/s12274-022-5244-z.
[19] C. Yi, Y. Yang, T. Zhang, X. Wu, W. Sun, L. Yi, *J. Clean Prod.* **2020**, *277*, 123585.
[20] J. Yang, E. Fan, J. Lin, F. Arshad, X. Zhang, H. Wang, F. Wu, R. Chen, L. Li, *ACS Appl. Energy Mater.* **2021**, *4*, 6261.
[21] H. Wang, Y. Huang, C. Huang, X. Wang, K. Wang, H. Chen, S. Liu, Y. Wu, K. Xu, W. Li, *Electrochim. Acta* **2019**, *313*, 423.
[22] Y. Yang, S. Song, S. Lei, W. Sun, H. Hou, F. Jiang, X. Ji, W. Zhao, Y. Hu, *Waste Manage.* **2019**, *85*, 529.
[23] H. Xiao, G. Ji, L. Ye, Y. Li, J. Zhang, L. Ming, B. Zhang, X. Ou, *J. Alloys Compd.* **2021**, *888*, 161593.
[24] Z. Ma, Y. Zhuang, Y. Deng, X. Song, X. Zuo, X. Xiao, J. Nan, *J. Power Sources* **2018**, *376*, 91.
[25] N. Cao, Y. Zhang, L. Chen, W. Chu, Y. Huang, Y. Jia, M. Wang, *J. Power Sources* **2021**, *483*, 229163.
[26] J. S. Edge, S. O'Kane, R. Prosser, N. D. Kirkaldy, A. N. Patel, A. Hales, A. Ghosh, W. Ai, J. Chen, J. Yang, S. Li, M.-C. Pang, L. B. Diaz, A. Tomaszewska, M. W. Marzook, K. N. Radhakrishnan, H. Wang, Y. Patel, B. Wubd, G. J. Offer, *Phys. Chem. Chem. Phys.* **2021**, *23*, 8200.
[27] J. P. Pender, G. Jha, D. H. Youn, J. M. Ziegler, I. Andoni, E. J. Choi, A. Heller, B. S. Dunn, P. S. Weiss, R. M. Penner, C. B. Mullins, *ACS Nano* **2020**, *14*, 1243.
[28] P. Zhang, T. Yuan, Y. Pang, C. Peng, J. Yang, Z.-F. Ma, S. Zheng, *J. Electrochem. Soc.* **2019**, *166*, A5489.
[29] D. Aurbach, M. D. Levi, E. Levi, A. Schechter, *J. Phys. Chem. B* **1997**, *101*, 2195.
[30] D. X. Luong, K. V. Bets, W. A. Algozeeb, M. G. Stanford, C. Kittrell, W. Chen, R. V. Salvatierra, M. Ren, E. A. McHugh, P. A. Advincula, Z. Wang, M. Bhatt, H. Guo, V. Mancevski, R. Shahsavari, B. I. Yakobson, J. M. Tour, *Nature* **2020**, *577*, 647.
[31] W. Chen, Z. Wang, K. V. Bets, D. X. Luong, M. Ren, M. G. Stanford, E. A. McHugh, W. A. Algozeeb, H. Guo, G. Gao, B. Deng, J. Chen, J. T. Li, W. T. Carsten, B. I. Yakobson, J. M. Tour, *ACS Nano* **2021**, *15*, 1282.

[32] M. G. Stanford, K. V. Bets, D. X. Luong, P. A. Advincula, W. Chen, J. T. Li, Z. Wang, E. A. McHugh, W. A. Algozeeb, B. I. Yakobson, J. M. Tour, *ACS Nano* **2020**, *14*, 13691.
[33] W. Chen, J. T. Li, Z. Wang, W. A. Algozeeb, D. X. Luong, C. Kittrell, E. A. McHugh, P. A. Advincula, K. M. Wyss, J. L. Beckham, M. G. Stanford, B. Jiang, J. M. Tour, *ACS Nano* **2021**, *15*, 11158.
[34] W. Chen, C. Ge, J. T. Li, J. L. Beckham, Z. Yuan, K. M. Wyss, P. A. Advincula, L. Eddy, C. Kittrell, J. Chen, D. X. Luong, R. A. Carter, J. M. Tour, *ACS Nano* **2022**, *16*, 6646.
[35] H. Yu, H. Dai, Y. Zhu, H. Hu, R. Zhao, B. Wu, D. Chen, *J. Power Sources* **2021**, *481*, 229159.
[36] H. Beyer, S. Meini, N. Tsiouvaras, M. Piana, H. A. Gasteiger, *Phys. Chem. Chem. Phys.* **2013**, *15*, 11025.
[37] P. A. Advincula, D. X. Luong, W. Chen, S. Raghuraman, R. Shahsavari, J. M. Tour, *Carbon* **2021**, *178*, 649.
[38] I. S. Zope, A. Dasari, Z.-Z. Yu, *Materials* **2017**, *10*, 935.
[39] B. Deng, X. Wang, D. X. Luong, R. A. Carter, Z. Wang, M. B. Tomson, J. M. Tour, *Sci. Adv.* **2022**, *8*, abm3132.
[40] C. Liu, Y. Li, D. Lin, P.-C. Hsu, B. Liu, G. Yan, T. Wu, Y. Cui, S. Chu, *Joule* **2020**, *4*, 1459.
[41] Z. Li, C. Li, X. Liu, L. Cao, P. Li, R. Wei, X. Li, D. Guo, K.-W. Huang, Z. Lai, *Energy Environ. Sci.* **2021**, *14*, 3152.
[42] S. Komaba, N. Kumagai, Y. Kataoka, *Electrochim. Acta* **2002**, *47*, 1229.
[43] W. Chen, R. V. Salvatierra, M. Ren, J. Chen, M. G. Stanford, J. M. Tour, *Adv. Mater.* **2020**, *32*, 2002850.
[44] G. Bouteau, A. N. Van-Nhien, M. Sliwa, N. Sergent, J.-C. Lepretre, G. Gachot, I. Sagaidak, F. Sauvage, *Sci. Rep.* **2019**, *9*, 135.
[45] M. B. Pinson, M. Z. Bazant, *J. Electrochem. Soc.* **2012**, *160*, A243.
[46] S. Jurng, Z. L. Brown, J. Kim, B. L. Lucht, *Energy Environ. Sci.* **2018**, *11*, 2600.
[47] W. Li, *J. Electrochem. Soc.* **2020**, *167*, 090514.
[48] C. Fang, J. Li, M. Zhang, Y. Zhang, F. Yang, J. Z. Lee, M. H. Lee, J. Alvarado, M. A. Schroeder, Y. Yang, B. Lu, N. Williams, M. Ceja, L. Yang, M. Cai, J. Gu, K. Xu, X. Wang, Y. S. Meng, *Nature* **2019**, *572*, 511.
[49] M. Ren, J. Zhang, J. M. Tour, *Carbon* **2018**, *139*, 880.
[50] S. Rattanaweeranon, P. Limsuwan, V. Thongpool, V. Piriyawong, P. Asanithi, *Procedia Eng.* **2012**, *32*, 1100.
[51] W. Chen, R. V. Salvatierra, J. T. Li, D. X. Luong, J. L. Beckham, V. D. Li, N. La, J. Xu, J. M. Tour, *Adv. Mater.* **2022**, *34*, 2202668.
[52] K. Zou, P. Cai, B. Wang, C. Liu, J. Li, T. Qiu, G. Zou, H. Hou, X. Ji, *Micro Nano Lett.* **2020**, *12*, 121.
[53] S. Han, *Sci. Rep.* **2019**, *9*, 5555.
[54] J. H. Park, H. Yoon, Y. Cho, C.-Y. Yoo, *Materials* **2021**, *14*, 4683.
[55] R. V. Salvatierra, G. A. Lopez-Silva, A. S. Jalilov, J. Yoon, G. Wu, A. L. Tsai, J. M. Tour, *Adv. Mater.* **2018**, *30*, 1803869.
[56] M. Wang, A. Elgowainy, U. Lee, A. Bafana, P. T. Benavides, A. Burnham, H. Cai, Q. Dai, U. R. Gracida-Alvarez, T. R. Hawkins, P. V. Jaquez, J. C. Kelly, H. Kwon, Z. Lu, X. Liu, L. Ou, P. Sun, O. Winjobi, H. Xu, E. Yoo, G. G. Zaimes, *Summary of Expansions and Updates in GREET 2020*, Lemont, IL, USA **2020**.
[57] Q. Dai, L. Gaines, J. Spangenberger, J. C. Kelly, S. Ahmed, M. Wang, Everbatt: A Closed-Loop Battery Recycling Cost and Environmental Impacts Model, **2020**, www.Anl.Gov/egs/everbatt (accessed: December 2022).
[58] X. Zhang, L. Li, E. Fan, Q. Xue, Y. Bian, F. Wu, R. Chen, *Chem. Soc. Rev.* **2018**, *47*, 7239.
[59] K. M. Wyss, R. D. D. Kleine, R. L. Couvreur, A. Kiziltas, D. F. Mielewski, J. M. Tour, *Commun. Eng.* **2022**, *1*, 3.
[60] D. Surovtseva, E. Crossin, R. Pell, L. Stamford, *J. Ind. Ecol.* **2022**, *26*, 964.
[61] P. Engels, F. Cerdas, T. Dettmer, C. Frey, J. Hentschel, C. Herrmann, T. Mirfabrikikar, M. Schueler, *J. Clean Prod.* **2022**, *336*, 130474.
[62] Y. Yao, K. K. Fu, S. Zhu, J. Dai, Y. Wang, G. Pastel, Y. Chen, T. Li, C. Wang, T. Li, L. Hu, *Nano Lett.* **2016**, *16*, 7282.
[63] Scaleup of FJH for graphene synthesis, see https://www.universal-matter.com/ (accessed: June 2022).
[64] J. M. Montes, F. G. Cuevas, J. Cintas, F. Fátima Ternero, E. S. Caballero, *Electrical and Electronic Properties of Materials*, IntechOpen, London, United Kingdom **2018**.
[65] Wolfram Research, Inc., Mathematica, Version 11.3, Champaign, IL, **2018**.
[66] COMSOL Multiphysics v. 5.5. www.comsol.com. COMSOL AB, Stockholm, Sweden.
[67] R. E. Taylor, H. Groot, Thermophysical Properties of Poco Graphite. A Report to Air Force Office of Scientific Research From Properties Research Laboratory, **1980**, https://www.osti.gov/etdeweb/biblio/6700249.
[68] Graphite Properties and Characteristics For Industrial Applications, **2020**, https://poco.entegris.com/content/dam/poco/resources/referencematerials/brochures/brochure-graphite-properties-and-characteristics-11043.pdf (accessed: July 2022).